



Influences of feed rate and wall thickness reduction on the microstructures of thin-walled Hastelloy C-276 cylindrical parts during staggered spinning

Y. C. Lin¹ · Shu-Sheng Qian¹ · Xiao-Min Chen² · Jun-Quan Wang¹ · Xin-He Li¹ · Hui Yang¹

Received: 31 July 2019 / Accepted: 23 December 2019 / Published online: 8 January 2020
© Springer-Verlag London Ltd., part of Springer Nature 2020

Abstract

Staggered spinning is an advanced method to manufacture thin-walled cylindrical parts. The microstructure evolution, which dominantly influences the overall performance, is very complex during the staggered spinning of Ni-based cylinder. In this work, the influences of feed rate and wall thickness reduction on the microstructures of a thin-walled Hastelloy C-276 cylinder during staggered spinning are investigated. It is found that the deformation of parts is highly inhomogeneous, and the microstructures are sensitive to the feed rate and wall thickness reduction during the staggered spinning. When the wall thickness reduction is small, the single slip is responsible for the deformation of grains. The deformation mechanism changes from single slip to cross slip with the increase of wall thickness reduction. Moreover, the uniform deformation of thin-walled Hastelloy C-276 cylinder can be obtained when the feed rate is about 0.8 mm/r or the wall thickness reduction is about 44.1%. These findings provide guidance for controlling the microstructures of thin-walled cylindrical parts during staggered spinning.

Keywords Alloy · Spinning · Thin-walled cylindrical parts · Microstructure evolution · Deformation mechanism

1 Introduction

As an economic and effective technology, the spinning forming is widely used to produce thin-walled cylindrical parts [1, 2]. It is usually classified into the backward and forward spinning according to whether the flow direction of material is same as that of roller feed [3–5]. Because of the constraints of staggered rollers, the forming precision of parts can be significantly improved during the backward staggered spinning [6–8]. However, the spinning parameters have great influence on the microstructures of cylindrical parts during the staggered spinning. Therefore, the effects of parameters on microstructure evolution during staggered spinning should be comprehensively investigated.

In past, some researchers have studied the microstructure evolution during the spinning of different parts. Xia et al. [9] found that the total wall thickness thinning ratio can promote the progress of DRX and refine the average grain size. Xiao et al. [10] found that the grain size increases slightly with the increased thinning ratio during the further power spinning of ASTM1020 steel. Hui et al. [11] found that the power spinning can significantly refine the initial equiaxed α grains in a Cu-Sn alloy. Cao et al. [12] claimed that the average grain size of spun AZ80 magnesium alloy tube obviously increases with the decreased thinning ratio. Xiao et al. [13] found that the dislocation slip combined with twinning is the dominant deformation mechanism during the spinning of ASTM 1020 tube. Xia et al. [14] found that the initial isometric grains of the spun ASTM 1020 tube are obviously stretched along axial direction. Molladavoudi et al. [15] concluded that the grain refinement becomes obvious with the increased wall thickness reduction in the spinning of 7075-O aluminum tube. Xiao et al. [16] researched that the average dynamic recrystallization (DRX) grain size of the hot spun Haynes 230 cylindrical parts decreases with the increased feed rate. Wang et al. [17] discovered that the volume fraction of α

✉ Y. C. Lin
yclin@csu.edu.cn; linyongcheng@163.com

¹ School of Mechanical and Electrical Engineering, Central South University, Changsha 410083, China

² College of Automotive and Mechanical Engineering, Changsha University of Science and Technology, Changsha 410114, China

grains decreases with the increased strain in the multi-pass spinning of a TA15 alloy. Maj et al. [18] claimed that the high density of dislocations induced in the spinning process can be effectively reduced after the aging heat treatment. Haghshenas and Klassen [19] found that the severe plastic deformation leads to the grain refinement and orientation in the axial direction of flow formed FCC alloys parts. Shan et al. [20] found that the grains in the external layer are elongated more severely than that in the internal layer during the spinning of Ti–6Al–2Zr–1Mo–1V tube. Bedekar et al. [21] suggested that the nanocrystalline grains can be obtained by the severe spinning plastic deformation in an AISI 1050 steel. Jahazi and Ebrahimi [22] implied that the cementite particles are obviously elongated in the spinning of D6ac steel. Tsivoulas et al. [23] found that the heterogeneous textures can be obtained along the axial direction in the spinning of Cr–Mo–V tubes. Mori et al. [24] concluded that the deformation of microstructure in the external layer is larger than that in internal layer in the spinning of cast aluminum parts. Zhang et al. [25] found that the grains become refined and uniform at the wall thickness reduction of 45% in the hot flow forming of AZ31B magnesium alloy. Haghshenas et al. [26] found that the grains are significantly elongated along the feed direction during the splined mandrel spinning of 5052 and 6061 aluminum alloys. Lee et al. [27] indicated that tangled dislocations and fibrous microstructure are formed in the spinning of C-250 maraging steels. Xu et al. [28] found that the fiber microstructure becomes more and more obvious with the increased thinning ratio during the hot spinning of a TA15 titanium alloy. Rasooli et al. [29] found that the grains were significantly elongated and refined along the feed direction in the spinning of 2024 aluminum alloy. Chi et al. [30] claimed that fine microstructure can be obtained by spinning TC11 alloy.

Because of its good corrosion resistance [31, 32], Hastelloy C-276 alloy is widely used in the rotor and stator shielding (RSS) of AP1000 nuclear reactor pumps [1, 33, 34]. The thin-walled spun RSS is a crucial part of nuclear reactor pump. Therefore, the forming qualities, such as microstructures and mechanical properties, are key concerns in the spinning process. In the authors' previous report [3], the influences of staggered spinning parameters on the dimensional accuracy of a thin-walled Hastelloy C-276 cylinder were investigated. However, during the spinning of cylindrical parts, the severe and non-uniform deformation usually occurs in parts, which easily induces the uneven microstructures and deteriorates the service performance. Hence, it is an important task to research the influences of spinning parameters on microstructures during the staggered spinning of thin-walled Hastelloy C-276 cylinders. In this work, the complex deformation mechanisms and microstructure evolution in the staggered

spinning process of a thin-walled Hastelloy C-276 cylinder were investigated, and the suitable spinning parameters are obtained. The experimental findings and conclusions are significant for the industrial staggered spinning of thin-walled Hastelloy C-276 cylindrical parts.

2 Experimental procedures

2.1 Material and staggered spinning process

In this study, the hot-rolled Hastelloy C-276 alloy was used. The chemical compositions (wt.%) is 0.5Co–15.60Cr–15.86Mo–3.20W–6.10Fe–0.04Si–0.60Mn–0.004C–(bal.) Ni. The geometric size of the thin-walled cylindrical billets is 299.60 mm (internal diameter) × 2 mm (wall thickness) × 300 mm (length). The main processing parameters are shown in Table 1. For most metallic materials, the roller feed rate is applicable in the range of 0.1–1.5 mm/r [12]. Considering the forming quality and efficiency, the values of roller feed rate were selected as 0.4 mm/r, 0.8 mm/r, 1.2 mm/r, and 1.6 mm/r. According to the authors' previous report [3], the values of wall thickness reduction were chosen as 37.4%, 44.1%, and 54.5%. The staggered spinning experiment (Table 2) was carried out on a CNC spinning machine, as depicted in Fig. 1.

2.2 Microstructure observations

In order to investigate the influence of spinning processing parameters on microstructures, the grain structures of the thin-walled spun cylinder were observed by optical microscope (OM) and transmission electron microscopy (TEM). Firstly, the specimens were cut from the spun parts, as shown in Fig. 2. For OM observations, the exposed external and internal surfaces (parallel to the direction of f) were polished and etched in a solution consisting of HCl (80 ml) + HNO₃ (4 ml) + CuCl₂ (2.5 g) + glycerin (20 g) at room temperature for 4–5 min.

Table 1 Main processing parameters used in staggered spinning

Parameters	Values
Fillet radius of rollers, $r_1/r_2/r_3$ (mm)	3/4/6
Attack angle of rollers, α (°)	20°
Sleeking angle of rollers, β (°)	3°
Diameter of rollers, D (mm)	300
Feed rates, f (mm/r)	0.4, 0.8, 1.2, 1.6
Axial staggered distances, a_{12}/a_{23} (mm)	3/4
Speed of Mandrel, n (rpm)	90
Wall thickness reductions, ψ	37.4%, 44.1%, 54%

Table 2 Experiments of staggered spinning

Case	Feed rate, f (mm/r)	Wall thickness reduction, ψ (%)
1	0.4	44.1
2	0.8	44.1
3	1.2	44.1
4	1.6	44.1
5	0.8	37.4%
6	0.8	54.5%

Figure 3 shows the microstructure of the Hastelloy C-276 alloy before staggered spinning. It is found that the microstructure is composed of equiaxed grains, and the mean grain size is 49.37 μm . For TEM observations, the discs, which have a diameter of 3 mm and thickness of 40~50 μm , near the external surface of the spun cylinder were electrochemically thinned in a mixed solution of 10% HClO_4 and 90% $\text{C}_2\text{H}_5\text{OH}$ with a voltage of 22 V at the temperature range of $-30\sim-25\text{ }^\circ\text{C}$.

In order to accurately characterize the microstructure evolution during staggered spinning, the volume fraction of broken grains and aspect ratio of grains are defined to illustrate the deformation characteristics of grains [35, 36]. The volume fraction of broken grain is calculated by the following:

$$X_{\text{bro}} = \frac{A_{\text{bro}}}{A_t} \tag{1}$$

where X_{bro} and A_{bro} are the volume fraction and volume of broken grains, respectively. A_t is the volume of the whole grains.

The aspect ratio of grains is calculated by the following:

$$R = \frac{L_{\text{maj}}}{L_{\text{min}}} \tag{2}$$

where R is aspect ratio (the aspect ratio) of the deformed grains, L_{maj} and L_{min} are the major and minor axes of

deformed grains, respectively.

The relative variations of X_{bro} and R in the external and internal surfaces have been calculated by Eqs. (3–4).

$$Re_X = \left| \frac{X_{\text{bro-ex}} - X_{\text{bro-in}}}{X_{\text{bro-ex}}} \right| \times 100\% \tag{3}$$

where $X_{\text{bro-ex}}$ and $X_{\text{bro-in}}$ are the volume fraction of broken grains in the external and internal surfaces, respectively. Re_X is the relative variations of X_{bro} in the external and internal surfaces.

$$Re_R = \left| \frac{R_{\text{ex}} - R_{\text{in}}}{R_{\text{ex}}} \right| \times 100\% \tag{4}$$

where R_{ex} and R_{in} are the aspect ratio of grains in the external and internal surfaces, respectively. Re_R is the relative variations of R in the external and internal surfaces.

3 Findings and discussion

3.1 Influences of feed rate on microstructures

3.1.1 Influences of feed rate on microstructures near external surface

Figure 4 depicts the influences of feed rate on the microstructures near external and internal surfaces of the spun cylinder. The sign f denotes the feeding direction of rollers during staggered spinning. Compared to the grains before spinning (Fig. 3), the equiaxed grains were obviously elongated along the feeding direction and some broken grains can be found after staggered spinning. Figure 4 a, c, and e show the influences of feed rate on the microstructures near the external surface of spun parts. It can be found that the elongation degree of grains and the number of broken grains firstly decreases and then increases with the increased feed rate. In order to accurately

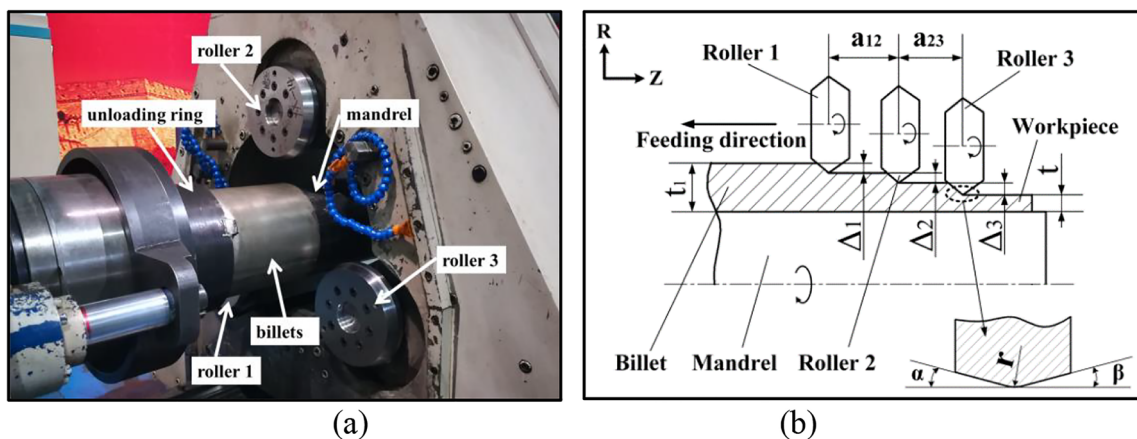


Fig. 1 Schematic of staggered spinning tests: **a** three-roller CNC spinning machine; **b** distribution of rollers

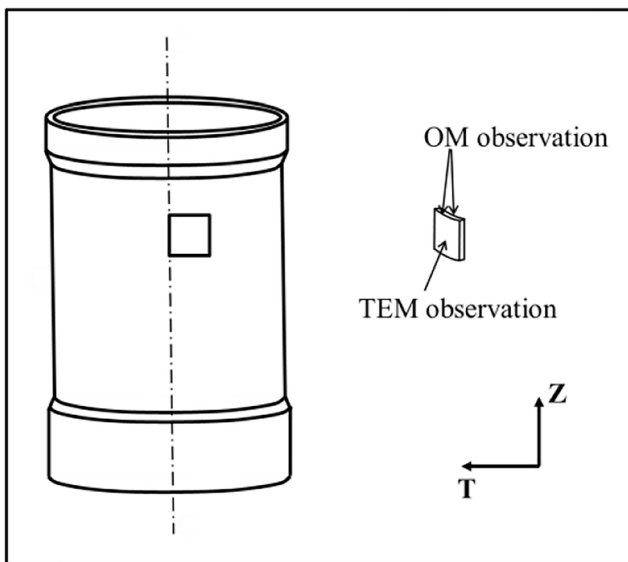


Fig. 2 Sampling from the spun thin-walled cylindrical parts for microstructure observations

define the deformation features of grains, the volume fraction of broken grains (X_{bro}), and aspect ratio (R) are evaluated according to Eqs. (1) and (2), respectively. Figure 5 a and c show the influences of feed rate on X_{bro} and R near the external surface of spun cylinder. Obviously, the volume fraction of broken grains and aspect ratio of the deformed grains both firstly drops and then rises with the increased feed rate.

According to the authors' previous research [1], the wall thickness of spun cylinder significantly increases with the increased feed rate, which suggests that the actual wall thickness reduction of spun cylinder is larger at a small feed rate. Therefore, the deformation of spun cylinder is more sufficient at a small feed rate. As a result, the elongation of grains becomes more obvious, and more broken grains can be found

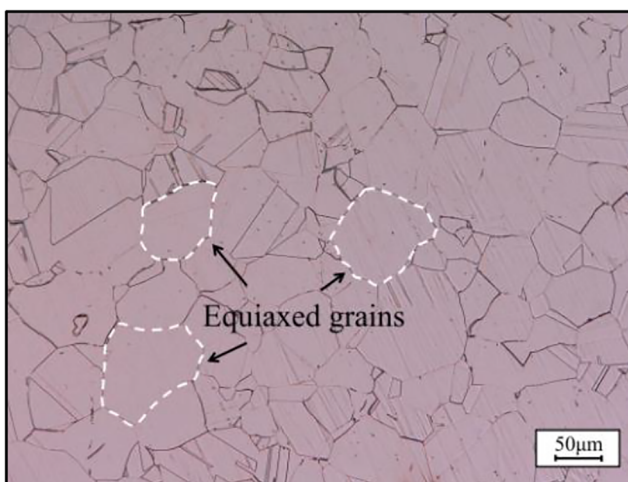


Fig. 3 The microstructure of Hastelloy C-276 alloy before staggered spinning

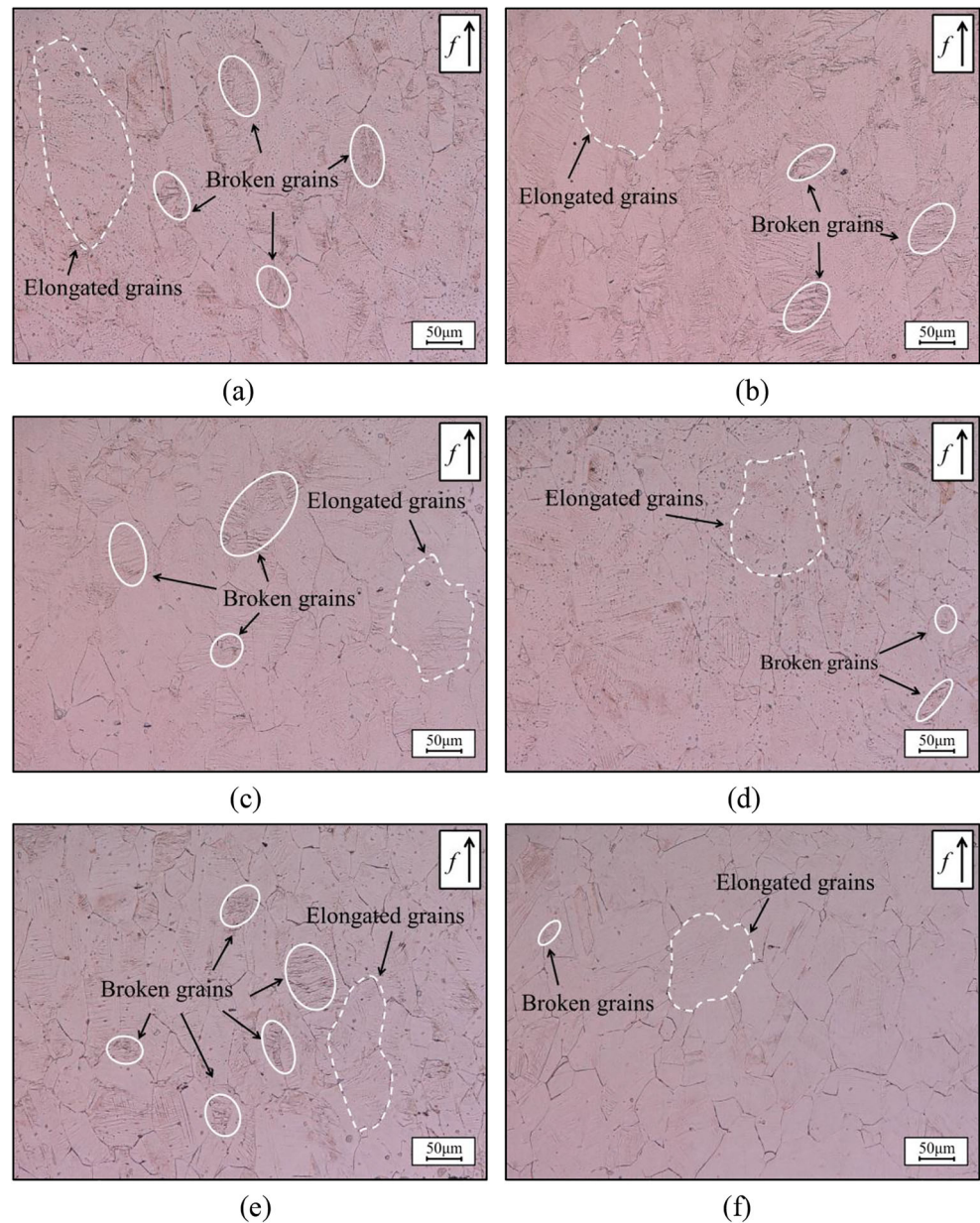
around grain boundaries. However, the plastic deformation of the cylindrical parts became very intense at a large feed rate. Here, the strain rate of the spun part was calculated by the method mentioned in Xiao's research [15]. Figure 6 shows the influences of feed rate on strain rate in the spun cylinder. It can be found that the strain rate in the spun cylinder significantly increases with the increase of feed rate. In the spinning process, the rollers are in contact with the external surface of the spun cylinder and rotate by the rolling friction with the billet. Thus, the friction is very small between the rollers and billet, and the strain rate significantly influences the deformation of cylindrical parts near external surface. Although the actual wall thickness reduction of spun cylinder is small at a large feed rate, the large strain rate near the external surface makes the severe plastic deformation, inducing the increase of X_{bro} and R . Consequently, the volume fraction of broken grains and the aspect ratio of deformed grains near the external surface both first decrease and then increase with the increased feed rate.

3.1.2 Influences of feed rate on microstructures near internal surface

Figure 4 b, d, and f show the influences of feed rate on the microstructures near the internal surface of spun cylinder. The detailed values of X_{bro} and R near the internal surface are shown in Fig. 5 b, d. Clearly, the values of X_{bro} and R near the internal surface both increase with the decreased feed rate. This is because the actual wall thickness reduction of spun cylinder is larger at lower feed rates. The deformation of spun cylinder is more sufficient when the feed rate is small. In the spinning process, the billet and the mandrel are fixed together to make sure the synchronous rotation, and the internal surface of spun cylinder is in contact with the mandrel by sliding friction. The friction between the mandrel and internal surface of thin-walled cylinder is distinctly much larger than that near the external surface. Thus, the influence of strain rate on the deformation near internal surface is much smaller than that near the external surface. The actual wall thickness reduction of spun cylinder obviously decreases with the increase of feed rate. Consequently, the deformation degree of spun cylinder decreases, and the values of X_{bro} and R near the internal surface decrease with the increased feed rate.

Also, it is clearly that the X_{bro} and R near the external surface are larger than those near the internal surface. This demonstrates that the deformation near the external surface of spun cylinder is more sufficient than that near the internal surface. Table 3 shows the effects of feed rate on Re_X and Re_R . It can be seen that the Re_X increases, but the Re_R first decreases and then increases with the increase of feed rate. Although the Re_X is lowest at the feed rate of 0.4 mm/r, but the value of Re_R is relatively large. When the feed rate is increased as 0.8 mm/r, the value of Re_X increases, but the Re_R dramatically decreases.

Fig. 4 Influences of feed rate on the microstructures of the spun thin-walled cylinder: **a** 0.8 mm/r—external surface; **b** 0.8 mm/r—internal surface; **c** 1.2 mm/r—external surface; **d** 1.2 mm/r—internal surface; **e** 1.6 mm/r—external surface; **f** 1.6 mm/r—internal surface



Moreover, the diameter growth easily occurs at small feed rates, which will reduce the forming quality of thin-walled spun parts [3]. So, the feed rate of 0.8 mm/r is favorable for the uniform deformation of the thin-walled cylinder during staggered spinning.

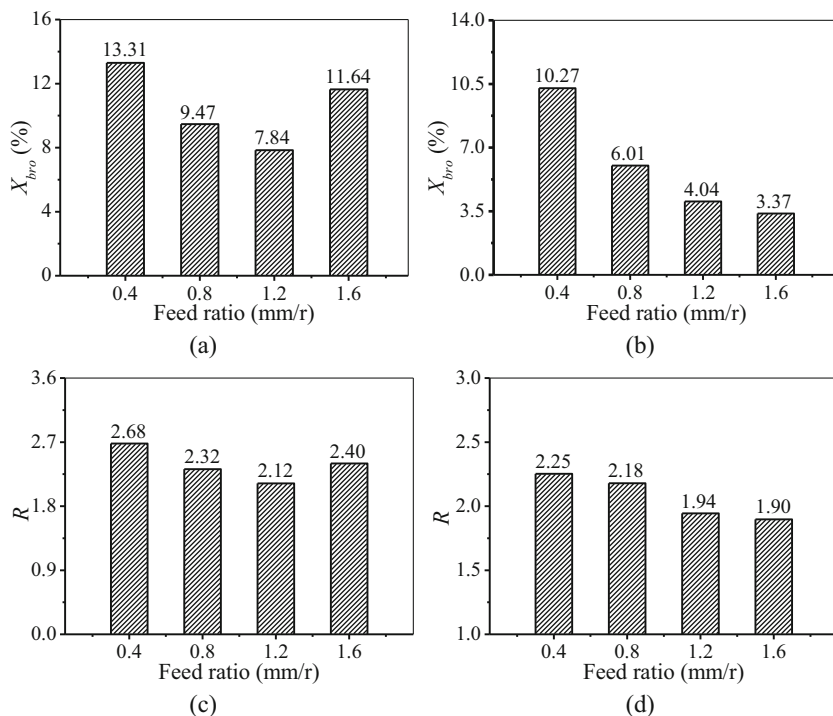
3.2 Influences of wall thickness reduction on microstructures

3.2.1 Influences of wall thickness reduction on microstructures near external surface

Figure 7 a and c show the influences of wall thickness reduction on the microstructures near the external surface

of spun cylinder. The microstructures near the external surface at the wall thickness reduction of 44.1% are shown in Fig. 4a. It can be found that the elongation degree of grains and the number of broken grains both decrease with the decreased wall thickness reduction. Figure 8 a and c show the influences of wall thickness reduction on X_{bro} and R near the external surface of spun cylinder. Obviously, the volume fraction of broken grains and aspect ratio of the deformed grains both decrease with the decreased wall thickness reduction. At a small wall thickness reduction, the deformation degree of spun cylinder is low, and the deformation of grains is not sufficient. Hence, the volume fraction of broken grains and aspect ratio of the deformed grains are small. With the increased wall thickness

Fig. 5 Influences of feed rate on X_{bro} and R of the spun thin-walled cylinder: **a** X_{bro} —external surface; **b** X_{bro} —internal surface; **c** R —external surface; **d** R —internal surface



reduction, the deformation of grains becomes more and more sufficient, and the volume fraction of broken grains and aspect ratio of the deformed grains increase at a large wall thickness reduction.

3.2.2 Influences of wall thickness reduction on microstructures near internal surface

Figure 7 b and d show the influences of wall thickness reduction on the microstructures near the internal surface of spun cylinder. The microstructures near the internal surface at the wall thickness reduction of 44.1% are shown in Fig. 4b, and the variations of X_{bro} and R near the internal surface with the wall thickness reduction are shown in Fig. 8a, c. It can be found that the elongation degree of grains and the number of

broken grains near the internal surface both decrease with the decrease of wall thickness reduction. This is because the deformation degree of the part decreases with the decrease of wall thickness reduction. Therefore, the X_{bro} and R near the internal surface is larger when a large wall thickness reduction is used.

Also, it is noticed that the X_{bro} and R near the external surface are large than those near the internal surface of spun cylinder. Table 4 shows the effects of wall thickness reduction on Re_X and Re_R . It can be seen that the Re_X and Re_R both decrease with the increase of wall thickness reduction. When the wall thickness reduction is increased from 37.4% to 44.1%, the Re_R significantly decreases and at a very low value. Although, the Re_X and Re_R are the lowest at the wall thickness reduction of 54.5%, but the bulge in front of roller easily appears when the wall thickness reaches 50%. It easily reduces the forming accuracy of thin-walled spun parts [1]. Consequently, the wall thickness reduction of 44.1% is favorable for the uniform deformation of the thin-walled cylinder during staggered spinning.

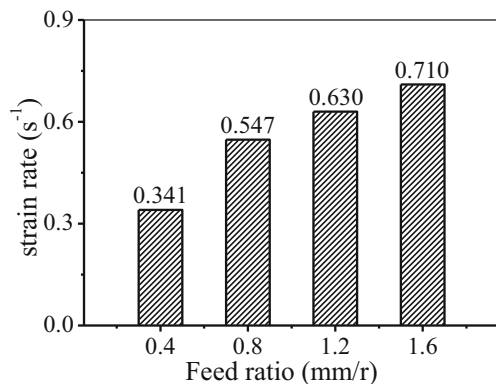


Fig. 6 Influences of feed rate on the strain rate of the spun thin-walled cylinder

Table 3 The effects of feed rate on Re_X and Re_R

f (mm/r)	Re_X (%)	Re_R (%)
0.4	22.84	16.04
0.8	36.54	6.03
1.2	48.46	8.49
1.6	71.05	20.8

Fig. 7 Influences of wall thickness reduction on the microstructure of the spun thin-walled cylinder: **a** 37.4%—external surface; **b** 37.4%—internal surface; **c** 54.5%—external surface; **d** 54.5%—internal surface

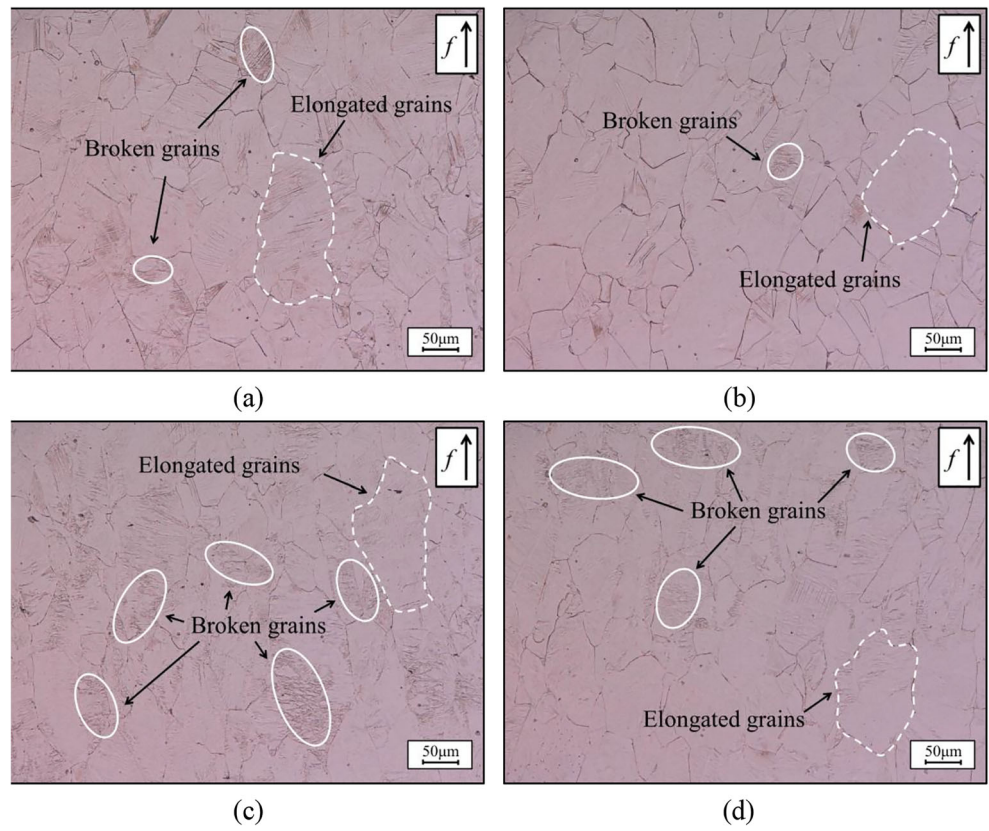


Fig. 8 Influences of wall thickness reduction on the microstructure of spun thin-walled cylinder: **a** X_{bro} —external surface; **b** X_{bro} —internal surface; **c** R —external surface; **d** R —internal surface

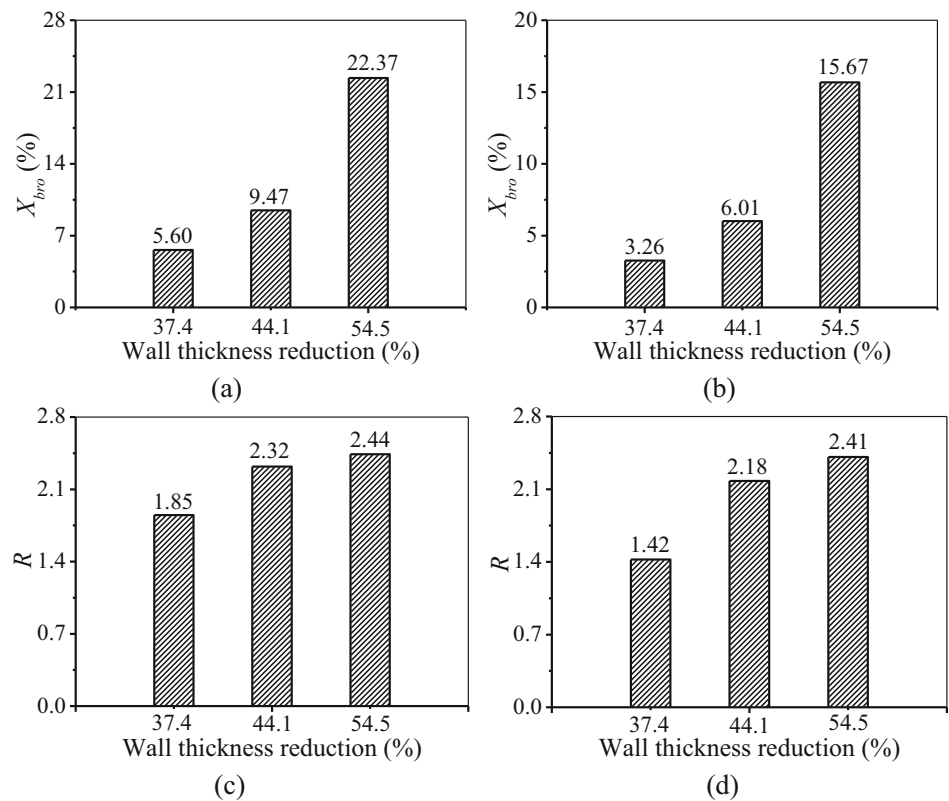


Table 4 The effect of wall thickness reduction on Re_X and Re_R

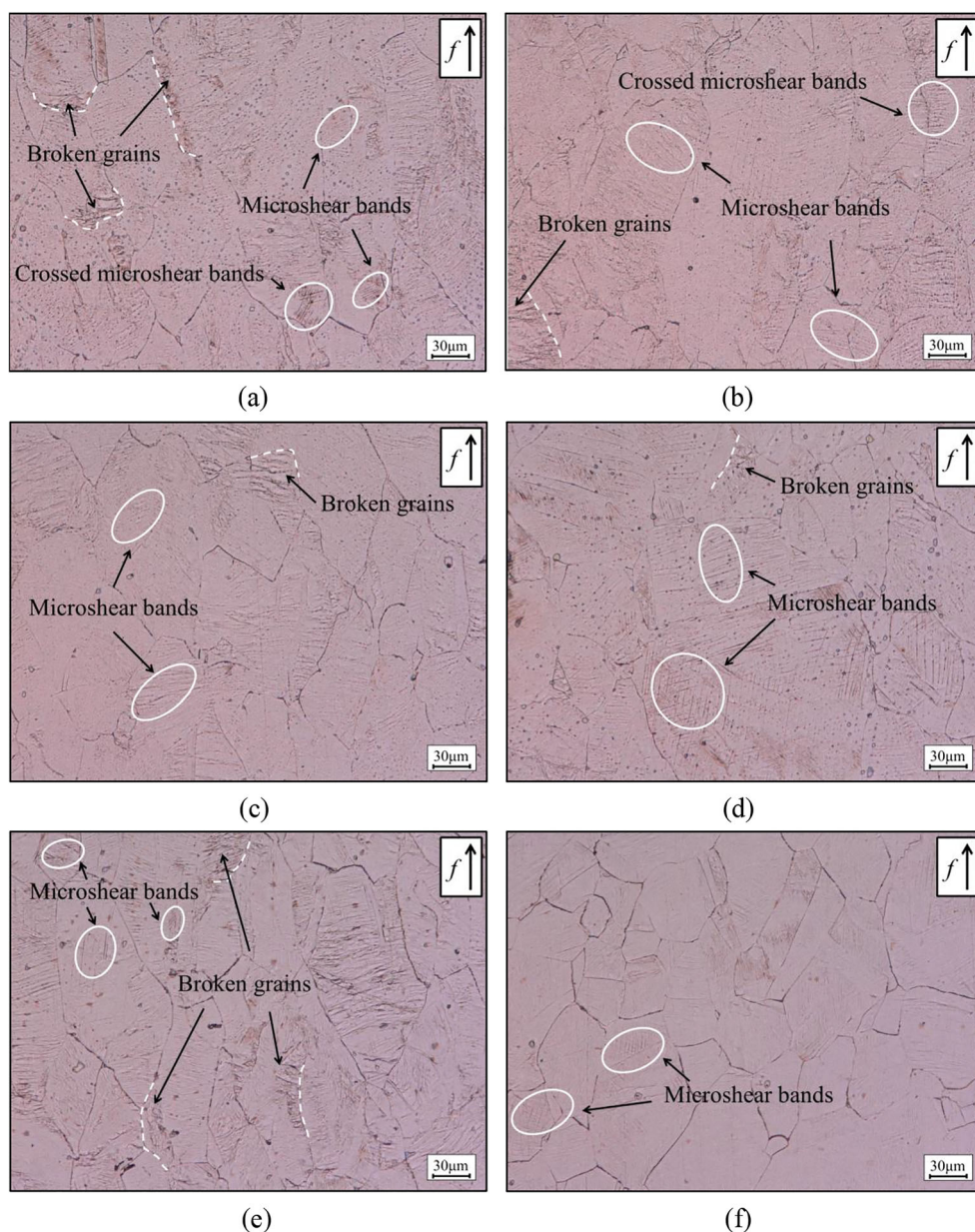
Ψ (%)	Re_X (%)	Re_R (%)
37.4	41.78	23.24
44.1	36.54	6.03
54.5	29.95	1.22

3.3 Microstructure evolution during staggered spinning

In order to further investigate the microstructure evolution of the thin-walled cylinder, the deformation features of grains is studied in details. Figure 9 presents the influences of feed rate on the deformation features of grains. After spinning, some

broken grains distributed around grain boundaries can be found, and there are lots of micro-shear bands in the deformed grains. Figure 9 a, c, and e depict the influences of feed rate on the deformation features of grains near the external surface of spun cylinder. It is found that the broken grains and micro-shear bands firstly decrease and then increase with the increased feed rate. In the spinning process, the shearing action of the roller and the mandrel on the cylinder makes it deformed and thinner. The stack fault energy of nickel base alloy is low. Thus, the slip is apt to occur during the deformation of spun parts. When the feed rate is small, the deformation of spun cylinder is more sufficient, and the shearing action of the roller and the mandrel is stronger. Hence, there are more broken grains and micro-shear bands in the deformed grains. The

Fig. 9 Influences of feed rate on the deformation feature of grains: **a** 0.8 mm/r—external surface; **b** 0.8 mm/r—internal surface; **c** 1.2 mm/r—external surface; **d** 1.2 mm/r—internal surface; **e** 1.6 mm/r—external surface; **f** 1.6 mm/r—internal surface

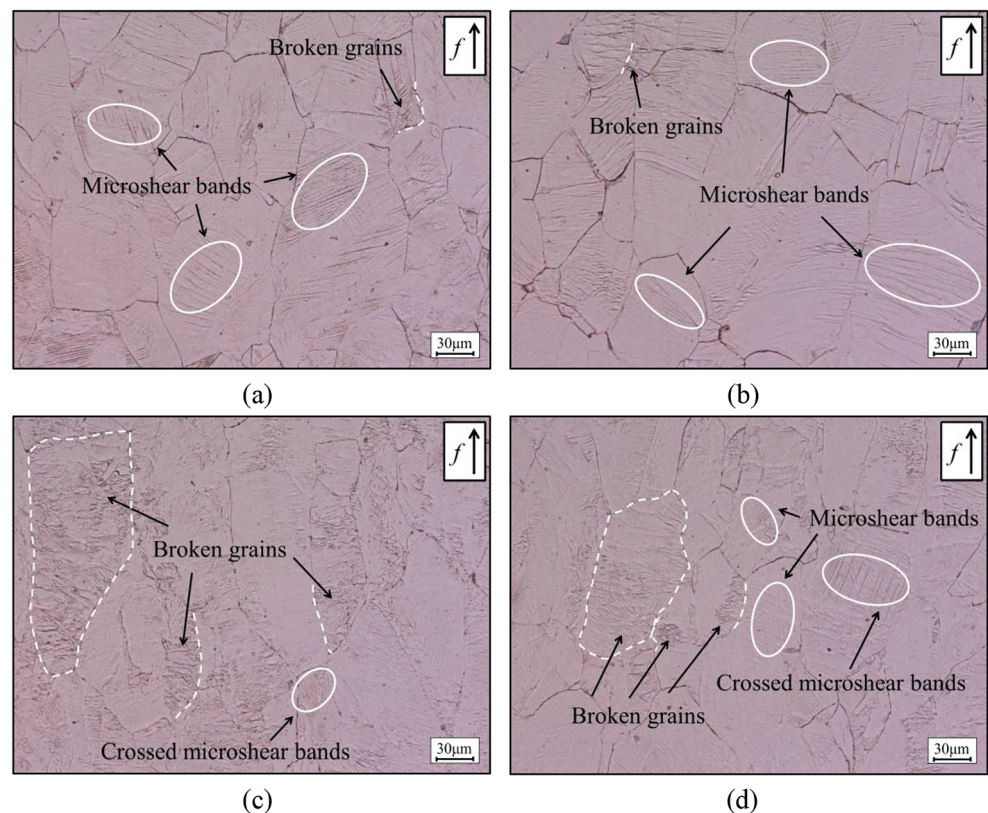


region of broken grains is large and some crossed micro-shear bands can be found within the elongated grains. The interaction of micro-shear bands, as well as the hindrance of grain boundaries, makes the grain broke along grain boundaries. With the increased feed rate, the deformation degree of spun cylinder decreases, and the shearing action of the roller and the mandrel on the cylinder becomes weaken. As a result, the number of broken grains and micro-shear bands decreases. As the feed rate is further increased, the strain rate near the external surface of spun cylinder significantly increases (Fig. 6), which increase the number of the broken grains and micro-shear bands again.

Figure 9 b, d, and f show the influences of feed rate on the deformation features of grains near the internal surface of spun cylinder. It is found that the number of the broken grains and micro-shear bands increase with the decreased feed rate. With the increased feed rate, the deformation degree of spun cylinder decreases and the shearing action of the roller and the mandrel on the cylinder becomes weaken. Consequently, the broken grains and micro-shear bands both increase with the decrease of feed rate. Meanwhile, it is found that the broken grains and micro-shear bands near the external surface are more than that near the internal surface of spun cylinder, which is consistent with the variations of X_{bro} and R , as observed in Fig. 8.

Figure 10 a and c show the influences of wall thickness reduction on the microstructures near the external surface of spun cylinder. The microstructures near the external surface at the wall thickness reduction of 44.1% are shown in Fig. 9a. It can be found that the number of broken grains and micro-shear bands in the deformed grains increase with the increased wall thickness reduction. The deformation degree of spun cylinder decreases with the decrease of wall thickness reduction, and the shearing action of the roller and the mandrel on the cylinder increases. Therefore, the broken grains and the micro-shear bands in the deformed grains are larger at a large wall thickness reduction. Figure 10 b and d show the influences of wall thickness reduction on the microstructures near the internal surface of spun cylinder. The microstructures near the internal surface at the wall thickness reduction of 44.1% are shown in Fig. 9b. It is noticed that the influences of wall thickness reduction on the deformation feature near the internal surface of spun cylinder are the same as the external surface. The number of the broken grains and micro-shear bands in the deformed grains near internal surface increase with the increased wall thickness reduction. In addition, when the wall thickness reduction is low, the micro-shear bands in the deformed grains are parallel to each other and the broken grains distribute around grain boundaries (Fig. 10a–b). With the increased wall thickness reduction, the region of broken grains

Fig. 10 Influences of wall thickness reduction on the microstructure of the spun thin-walled cylinder: **a** 37.4% - external surface; **b** 37.4%—internal surface; **c** 54.5%—external surface; **d** 54.5%—internal surface



enlarges and some crossed micro-shear bands can be found in the elongated grains (Fig. 9a–b). When the wall thickness reduction is further increased, the hindrance of grain boundaries on the micro-shear bands dramatically increases, which leads to the extension of grain breakage from the boundary to the interior of grains. As a result, the initial equiaxed grains are broken into small grains, as illustrated in Fig. 10c–d.

3.4 Deformation mechanisms of the thin-walled cylindrical parts during staggered spinning

Figure 11 depicts the TEM observations of the spun thin-walled cylinder near the external surface at different feed rates. A mass of dislocations and shear planes can be found in the deformed grains in the spun cylinder. When the feed rate is 0.4 mm/r (Fig. 11a), there are high densities dislocations in the deformed grains, and a large area of dislocation tangle zones (DTZs) and dislocation cells (DCs) can be easily found. Besides, the shear planes cross with each other and DTZs are hindered and accumulate around these shear planes, and some subgrains formed near the shear planes. The angle of the crossed shear planes were measured and marked in the TEM photographs. From Fig. 11a, c, it can be found that the angle of

the crossed shear planes first increases and then decreases with the increased feed rate, and the crossed shear planes transform into parallel at the feed rate of 1.2 mm/r. In addition, the dislocation density also first increases and then decreases with the increased feed rate. DTZs and DCs can be hardly seen in the deformed grains at the feed rate of 1.2 mm/r. When the feed rate is further increased (Fig. 11d), the dislocation density increases again, and DTZs and DCs can be easily found in deformed grains. Moreover, the parallel shear planes transform into crossed ones, and some subgrains can be found near these shear planes. The deformation degree of the cylinder decreases with the increased feed rate. Thus, the shearing action of the roller and the mandrel on the cylinder decreases. As a result, the dislocation density decreases and the angle of the crossed shear planes increases with the increased feed rate. There are fewer subgrains formed around the shear planes. However, with the further increased feed rate, the strain rate near external surface of spun cylinder significantly increases, which leads to an increase in dislocation again and facilitates the formation of subgrains along the shear planes.

Figure 12 shows the TEM observations of the spun thin-walled cylinder in external surface at different wall thickness reductions. The TEM observations near the external surface at

Fig. 11 TEM observations of the spun cylinder near the external surface: **a** 0.4 mm/r; **b** 0.8 mm/r; **c** 1.2 mm/r; **d** 1.6 mm/r

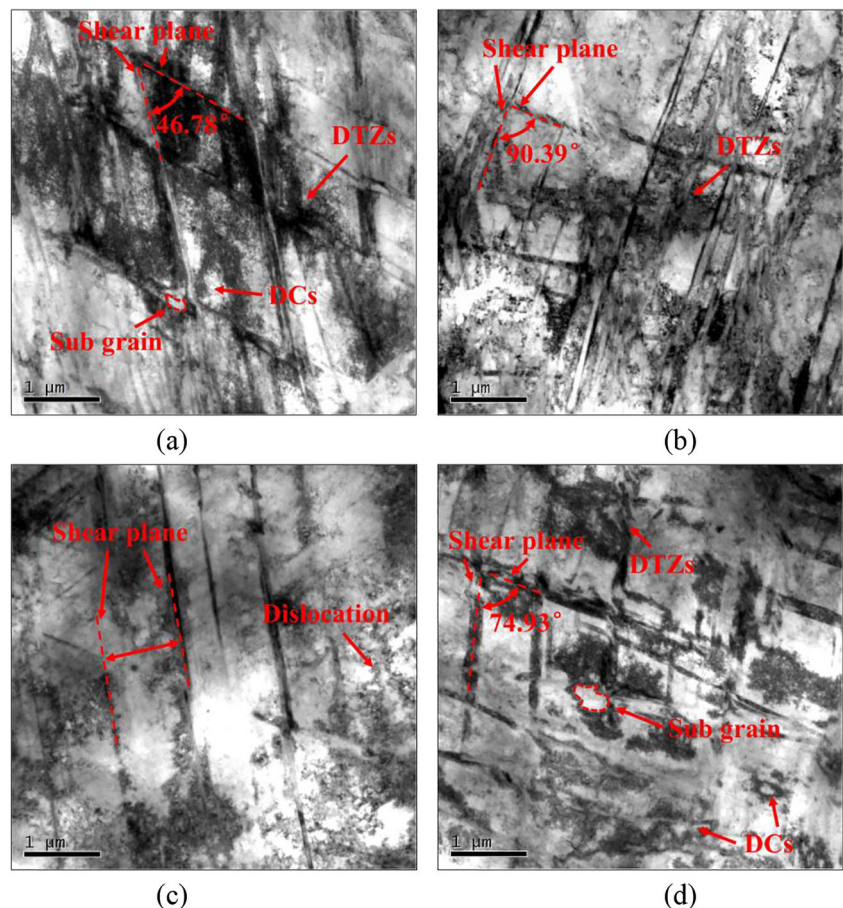
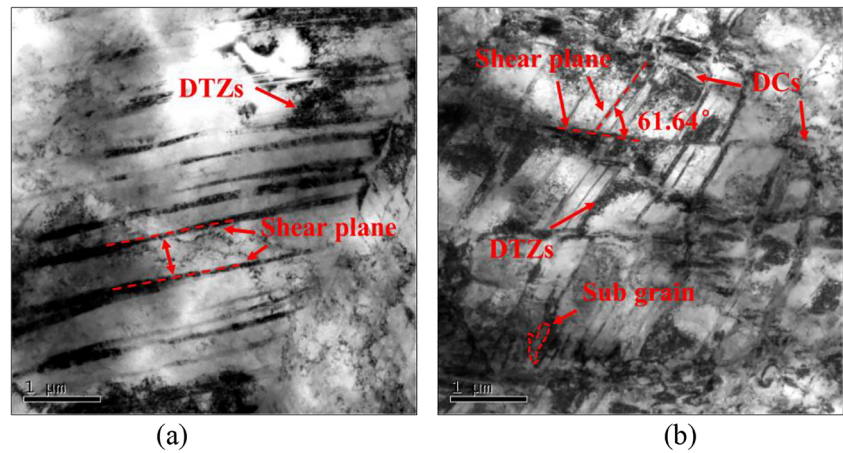


Fig. 12 Influences of wall thickness reduction on the microstructures of the spun cylinder: **a** 37.4%; **b** 54.5%



the wall thickness reduction of 44.1% are shown in Fig. 11b. It is clearly that the dislocation density obviously decreases with the decreased wall thickness reduction. When wall thickness reduction is 37.4%, the dislocation density in the deformed grains is low and the region of DTZs is very small. The shear planes are parallel with each other. The dislocation density significantly increases and large region of DTZs can be found around the shear planes with the increased wall thickness reduction. The shear planes change from parallel to cross. The region of DTZs increases and DCs can be easily found in the deformed grains with the further increased wall thickness reduction. In addition, the angle of crossed shear planes decreases and some subgrains can be found along the shear planes. With the increased wall thickness reduction, the deformation degree of spun parts increases and the shearing action of the roller and the mandrel on the cylinder become strong. Hence, the dislocation density significantly increases and the angle of the shear planes decreases with the increased wall thickness reduction.

Figure 13 shows the microstructure evolution scheme of the thin-walled cylinder during staggered spinning. The microstructure evolution near the external and internal surfaces of spun cylinder is different. Before staggered spinning, the microstructures in the billet are uniform equiaxed grains. The grains are obviously elongated in the feeding direction in the spinning process. Because of the different friction states on the internal and external surfaces of spun cylinder, the grains near the external surface has larger volume fraction of broken grains and aspect ratio compared to the internal surface, as shown in Fig. 13. So, the deformation of spun parts during staggered spinning is not uniform in the radial direction, and the deformation degree near the external surface is larger than that near internal surface.

The wall thickness of spun parts significantly decreases with the decreased feed rate [1], which means the actual wall thickness reduction is larger at a small feed rate. So, the influence of feed rate and wall thickness reduction can be unified

as that of wall thickness reduction. As shown previously, although the microstructures near the external and internal surfaces of spun cylinder are different, the evolution processes of microstructures are almost the same. Therefore, the microstructure evolution can be illustrated by taking the external surface as an example, as shown in Fig. 14. Figure 14 a shows the initial microstructures of the billets; it can be found that the microstructures in the billet are uniform equiaxed grains before staggered spinning. After staggered spinning, the grains are elongated along the feeding direction, and a single slip occurs in most crystals. A few broken grains appear near grain boundary because of the hindrance of grain boundary to micro-shear bands, as shown in Fig. 14b. With the increased wall thickness reduction, the shearing action of the roller and the mandrel on the cylinder increases. The grains are elongated along the feeding direction, and the single slip gradually changes to cross slip. More and more grains break around grain boundaries due to the hindrance of grain boundary to micro-shear bands, as shown in Fig. 14c. With the further increased wall thickness reduction, the grains are further

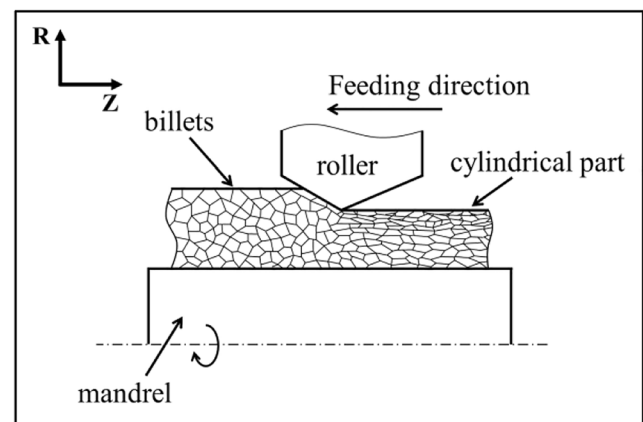
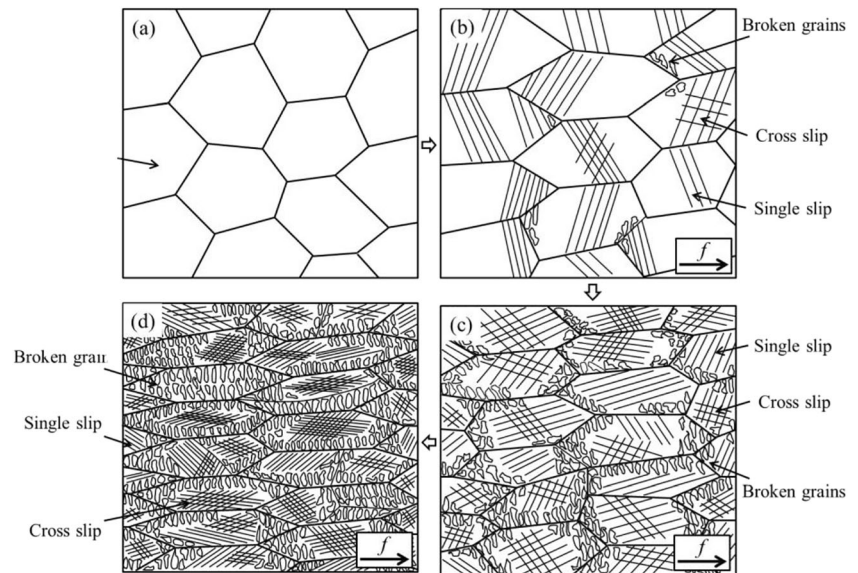


Fig. 13 The microstructure evolution scheme of the thin-walled cylinder during staggered spinning

Fig. 14 The microstructure evolution of the thin-walled cylinder during staggered spinning



elongated, and the cross slip becomes the main deformation mechanism. The grain breakage extends from the boundary to the interior of grains, as shown in Fig. 14d. Consequently, the initial equiaxed grains are broken into some small grains.

4 Conclusions

In this research, the microstructure evolution of thin-walled cylindrical parts during staggered spinning is investigated. The influences of spinning parameters on the microstructures of spun cylinder, as well as the deformation mechanisms, are analyzed. Some conclusions can be made as follows:

- 1) The deformation of the spun cylinder is not uniform in the radial direction. Meanwhile, the volume fraction of broken grains (X_{bro}) and aspect ratio of the deformed grains (R) near the external surface are larger than those near the internal surface.
- 2) The influences of feed rate and wall thickness reduction on the microstructures of spun cylinder are significant. With the increased feed rate, X_{bro} and R near the external surface firstly decrease and then increase, but X_{bro} and R near the internal surface decrease. With the increased wall thickness reduction, X_{bro} and R near the external and internal surfaces decrease. The feed rate of 0.8 mm/r or wall thickness reduction of 44.1% is favorable for the uniform deformation of the thin-walled cylinder during staggered spinning.
- 3) The influence of feed rate and wall thickness reduction on the deformation mechanisms can be unified as that of wall thickness reduction. When the wall thickness reduction is small, the single slip is the major deformation mechanism, and the grains initially break

around grain boundaries because of its hindrance on the micro-shear bands. With the increased wall thickness reduction, the deformation of grains changes from single slip to cross slip, and the grain breakage extends from the boundary to the interior of grains.

Funding information This work was supported by the National Natural Science Foundation of China of China (Grant No. 51775564), 973 programs (No.2015CB057305), and the Fundamental Research Funds for the Central Universities of Central South University (Grant No. 173711033), China.

Compliance with ethical standards

Conflict of interest The authors declare that they have no conflicts of interest.

References

1. Wong CC, Dean TA, Lin J (2003) A review of spinning, shear forming and flow forming processes. *Int J Mach Tools Manuf* 43(14):1419–1435
2. Jia Z, Han Z, Liu B, Fan Z (2017) Numerical simulation and experimental study on the non-axisymmetric die-less shear spinning. *Int J Adv Manuf Technol* 92(1–4):497–504
3. Lin YC, Qian SS, Chen XM, Li XH, Yang H (2019) Staggered spinning of thin-walled Hastelloy C-276 cylindrical parts: numerical simulation and experimental investigation. *Thin Wall Struct* 140:466–476
4. Zoghi H, Arezoodar AF, Sayeafabi M (2012) Effect of feed and roller contact start point on strain and residual stress distribution in dome forming of steel tube by spinning at an elevated temperature. *Proc IME B J Eng Manuf* 226(11):1880–1890
5. Zhang Q, Zhang C, Zhang MJ, Zhu CC, Fan SQ, Zhao SD (2015) Research of net-shape power spinning technology for poly-v grooved aluminum pulley. *Int J Adv Manuf Technol* 81(9–12):1601–1618

6. Wang J, Ge T, Lu GD, Li F (2016) A study of 3D finite element modeling method for staggered spinning of thin-walled tube. *J Zhejiang Univ Sci A* 17(8):646–666
7. Zhan M, Zhang T, Yang H, Li LJ (2016) Establishment of a thermal damage model for Ti-6Al-2Zr-1Mo-1V titanium alloy and its application in the tube rolling-spinning process. *Int J Adv Manuf Technol* 87(5–8):1345–1357
8. Sivanandini M, Dhani SS, Pabla BS (2012) Flow forming of tubes—a review. *Int J Sci Eng Res* 3(5):1–11
9. Xiao GF, Xia QX, Cheng XQ, Zhou YJ (2015) Research on the grain refinement method of cylindrical parts by power spinning. *Int J Adv Manuf Technol* 78(5–8):971–979
10. Xiao GF, Xia QX, Long JC, Chen WP (2018) Research on the forming quality and mechanical properties of cylindrical spun parts with ultrafine-grained structure during power spinning. *Int J Adv Manuf Technol* 97:2979–2986
11. Hui J, Feng Z, Fan WX, Yuan X (2018) The influence of power spinning and annealing temperature on microstructures and properties of Cu-Sn alloy. *Mater Charact* 144:611–620
12. Cao Z, Wang FH, Wan Q, Zhang ZY, Jin L, Dong J (2015) Microstructure and mechanical properties of AZ80 magnesium alloy tube fabricated by hot flow forming. *Mater Des* 67:64–71
13. Xiao GF, Xia QX, Cheng XQ, Long H (2016) New forming method of manufacturing cylindrical parts with nano/ultrafine grained structures by power spinning based on small plastic strains. *Sci China Tech Sci* 59(11):1656–1665
14. Xia QX, Xiao GF, Long H, Cheng XQ, Yang BJ (2014) A study of manufacturing tubes with nano/ultrafine grain structure by staggered spinning. *Mater Des* 59:516–523
15. Molladavoudi HR, Djavanroodi F (2011) Experimental study of thickness reduction effects on mechanical properties and spinning accuracy of aluminum 7075-O, during flow forming. *Int J Adv Manuf Technol* 52(9–12):949–957
16. Xiao GF, Zhu NY, Long JC, Xia QX, Chen WP (2018) Research on precise control of microstructure and mechanical properties of Ni-based superalloy cylindrical parts during hot backward flow spinning. *J Manuf Process* 34:140–147
17. Wang XX, Zhan M, Gao PF, Zhang HR (2018) Micromechanical behaviour of TA15 alloy cylindrical parts processed by multi-pass flow forming. *Mater Sci Eng A* 737:328–335
18. Maj P, Błyskun P, Kut S, Romelczyk-Baishya B, Mrugała T, Adamczyk-Cieslak B, Mizer J (2018) Flow forming and heat-treatment of Inconel 718 cylinders. *J Mater Process Technol* 253:64–71
19. Haghshenas M, Klassen RJ (2015) Mechanical characterization of flow formed FCC alloys. *Mater Sci Eng A* 641:249–255
20. Shan DB, Yang GP, Xu WC (2009) Deformation history and the resultant microstructure and texture in backward tube spinning of Ti-6Al-2Zr-1Mo-1V. *J Mater Process Technol* 209(17):5713–5719
21. Bedekar V, Pauskar P, Shivpuri R, Howe J (2014) Microstructure and texture evolutions in AISI 1050 steel by flow forming. *Procedia Eng* 81:2355–2360
22. Jahazi M, Ebrahimi G (2000) The influence of flow-forming parameters and microstructure on the quality of a D6ac steel. *J Mater Process Technol* 103(3):362–366
23. Tsivoulas D, da Fonseca JQ, Tuffs M, Preuss M (2017) Measurement and modelling of textures in flow formed Cr-Mo-V steel tubes. *Mater Sci Eng A* 685:7–18
24. Mori KI, Ishiguro M, Isomura Y (2009) Hot shear spinning of cast aluminium alloy parts. *J Mater Process Technol* 209(7):3621–3627
25. Zhang Y, Wang F, Dong J, Jin L, Liu C, Ding W (2018) Grain refinement and orientation of AZ31B magnesium alloy in hot flow forming under different thickness reductions. *J Mater Sci Technol* 34(7):1091–1102
26. Haghshenas M, Wood JT, Klassen RJ (2012) Investigation of strain-hardening rate on splined mandrel flow forming of 5052 and 6061 aluminum alloys. *Mater Sci Eng A* 532:287–294
27. Lee YJ, Kung MC, Lee IK, Chou CP (2007) Effect of lath microstructure on the mechanical properties of flow-formed C-250 maraging steels. *Mater Sci Eng A* 454:602–607
28. Xu WC, Shan DB, Wang ZL, Yang GP, Lu Y, Kang DC (2007) Effect of spinning deformation on microstructure evolution and mechanical property of TA15 titanium alloy. *Trans Nonferrous Met Soc China* 17(6):1205–1211
29. Rasooli M, Moshref-javadi M, Taherizadeh A (2015) Investigation of ultrasonic vibration effects on the microstructure and hardness of aluminum alloy 2024 tube spinning parts. *Int J Adv Manuf Technol* 77(9–12):2117–2124
30. Chi JX, Cai ZY, Li LL (2018) Optimization of spinning process parameters for long thin-walled cylinder of TC11 alloy based on processing map. *Int J Adv Manuf Technol* 97(5–8):1961–1969
31. Zhang C, Zhang LW, Shen WF, Li MF, Gu SD (2015) Characterization of hot deformation behavior of Hastelloy C-276 using constitutive equation and processing map. *J Mater Eng Perform* 24(1):149–157
32. Zhang C, Zhang LW, Shen WF, Liu CR, Xia YN (2016) The kinetics of metadynamic recrystallization in a Ni-Cr-Mo-based superalloy Hastelloy C-276. *J Mater Eng Perform* 25(2):545–552
33. Jaladurgam NR, Kanjarla AK (2018) Hot deformation characteristics and microstructure evolution of Hastelloy C-276. *Mater Sci Eng A* 712:240–254
34. Huang YC, Liu C, Xiao ZB (2018) Hot tensile deformation and fracture behaviours of Hastelloy C-276 alloy. *Mater Sci Technol* 34(5):620–627
35. Wang Q, Yang P, Zhang B, Fan H, Xu X, Li W, Ding H (2019) Microstructure and texture evolution of cold rolled 1070 Al alloy during the subsequent annealing treatment. *Results Phys* 13:102178
36. Shen YF, Guan RG, Zhao ZY, Misra RDK (2015) Ultrafine-grained Al-0.2 Sc-0.1 Zr alloy: the mechanistic contribution of nano-sized precipitates on grain refinement during the novel process of accumulative continuous extrusion. *Acta Mater* 100:247–255

Publisher's note Springer Nature remains neutral with regard to jurisdictional claims in published maps and institutional affiliations.